Multiobjective Optimization in 5G Hybrid Networks

Muhammad Shahmeer Omar, *Member, IEEE*, Syed Ali Hassan, *Senior Member, IEEE*, Haris Pervaiz, *Member, IEEE*, Qiang Ni, *Senior Member, IEEE*, Leila Musavian, *Member, IEEE*, Shahid Mumtaz, *Senior Member, IEEE*, and Octavia A. Dobre, *Senior Member, IEEE*

***Abstract*—The increasing adoption of the Internet of Things has led to the need for systems with higher spectral and energy efficiency (EE) in order to enable communication. Larger data rate demands had led researchers to look at millimeter wave (mmWave) bands to boost network rates. This paper investigates the downlink performance of a three-tier heterogeneous network that consists of sub-6 GHz macrocells overlaid with small cells operating on both the mmWave and sub-6 GHz bands. A model is developed using tools from stochastic geometry to analyze the coverage, rate, area spectral efficiency, and EE of such a network. Various deployment strategies and their impacts on the considered metrics are studied. Simulation results are used to verify the validity of the proposed model.**

***Index Terms*—Blockage models, fifth generation (5G), hybrid heterogeneous networks (HetNets), Internet of Things (IoT), millimeter wave, stochastic geometry.**

I. Introduction

THE EXPONENTIAL growth in recent traffic requirements has led to the need for new technologies to augment current network capacity. This coupled with congestion in the existing spectrum has led researchers to investigate the viability of previously unused frequency bands, such as the millimeter wave (mmWave) band. The deployment of mmWave base stations (BSs) operating at 10–300 GHz frequency bands [1] with available bandwidths of 2 GHz or more is considered a key enabler to achieve higher spectral and energy efficiency (EE) in fifth generation (5G) networks [2]–[5].

The use of mmWave transmissions was not considered feasible in the past due to various factors, such as greater pathloss and severe penetration losses. Experimental measurements using directional antennas [1], show that blockages cause substantial differences in the line-of-sight (LoS) and non LoS (NLoS) pathloss characteristics [6]. The higher pathloss restricts the cell sizes in mmWave networks, however, smaller wavelengths allow large antenna arrays to be packed in relatively small areas which makes transmit and receive beamforming more viable.

The performance of standalone mmWave cellular networks have been investigated in prior works [7]–[9] using insights from the propagation channel measurements. Rangan *et al.* [7] showed that mmWave networks are predominantly noise limited, while sub-6 GHz networks are interference-limited. Rangan *et al.* [7] proposed analytical blockage models for dense urban areas using various curve fitting techniques. However, these approaches lack the flexibility to be applied to diverse scenarios, such as a rural setting. In [8], the SINR and rate coverage trends of a standalone mmWave network were investigated by using real building locations of the Manhattan and Chicago regions. The authors also presented a comparison of real-world blockages with different blockage models. Bai and Heath [9] used stochastic geometry to analyze coverage and rate trends in standalone mmWave networks by deploying BSs using the Poisson point process (PPP). However, in these works, networks in which sub-6 GHz and mmWave BSs co-exist are not analyzed.

Most of the existing works in literature have focused on coverage and rate trends in UHF networks using stochastic geometry. For example, the work in [10] derives tractable expressions for coverage and rate in a network with general fading. The authors in [11]–[14] analyzed multitier heterogeneous networks (HetNets). Predictions of site specific performance are given in [15]. However, the models proposed in [11]–[15] are not directly applicable to mmWave communications due to the difference in propagation characteristics. Several recent studies, such as [16]–[20] have presented analytical frameworks to investigate the coverage and rate trends for the co-existing mmWave and sub-6 GHz networks.

Multiobjective optimization has been previously used for various problems in wireless communications. Bedeer *et al.* [21] and Amin *et al.* [22] used it for optimization in cognitive radio networks and to optimize the spectral and EE. However, there is little work that uses these techniques for mmWave HetNets.

The use of high gain directional antennas opens up the possibility of relaying in mmWave networks without significantly increasing the interference. Zhang *et al.* [23] analyzed the

Manuscript received September 12, 2017; revised November 30, 2017; accepted December 18, 2017. Date of publication December 29, 2017; date of current version June 8, 2018. This work was supported in part by the U.K. EPSRC under Grant EP/N032268/1. *(Corresponding author: Muhammad Shahmeer Omar.)*

M. S. Omar and S. A. Hassan are with the School of Electrical Engineering and Computer Science, National University of Sciences and Technology, Islamabad 44000, Pakistan (e-mail: 11beemomar@seecs.edu.pk; ali.hassan@seecs.edu.pk).

H. Pervaiz is with the 5G Innovation Center, University of Surrey, Guildford GU2 7XH, U.K. (e-mail: h.pervaiz@surrey.ac.uk).

Q. Ni is with the School of Computing and Communications, Lancaster University, Lancaster LA1 4WA, U.K. (e-mail: q.ni@lancaster.ac.uk).

L. Musavian is with the School of Computer Science and Electronic Engineering, University of Essex, Colchester CO4 3SQ, U.K. (e-mail: leila.musavian@essex.ac.uk).

S. Mumtaz is with the Instituto de Telecommuniições, DETI, Universidade de Aveiro, Aveiro 4554, Portugal (e-mail: smumtaz@av.it.pt).

O. A. Dobre is with the Department of Electrical and Computer Engineering, Memorial University, St. John's, NL A1B 3X5, Canada (e-mail: odobre@mun.ca).

Digital Object Identifier 10.1109/JIOT.2017.2788362

use of nonorthogonal multiple access, coupled with mmWave relaying to improve the coverage and rate performance. Zhang *et al.* [24] discussed the use of cooperative multicasting for multimedia transmissions. Relaying can have significant impact for coverage in indoor mmWave networks, where there are denser blockages. Yang *et al.* [25] used relaying to bypass obstacles and hence improve coverage.

In this paper, we introduce a tractable model for the analysis of a three-tier HetNet that consists of both mmWave and sub-6 GHz BSs. We use this model to analyze the coverage, rate, area spectral efficiency (ASE) and EE of the network. We also investigate several tradeoffs between the considered metrics and discuss optimal deployment strategies.

II. Contribution and Organization

In contrast to prior works [9]–[17], this paper extends the existing models of HetNets to incorporate mmWave small cells and analyzes the performance of the proposed network model using various metrics for disparate propagation environments, like coverage probability, rate, ASE, and EE. In particular, the main contributions of this paper are as follows.

1) We propose a tractable stochastic geometric approach to perform the analysis of the downlink transmission scheme of mmWave/sub-6 GHz hybrid 3-tier HetNets. We model the received SINR distributions at the user to derive the analytical expressions for tier association and coverage/outage probability in mmWave/sub-6 GHz hybrid HetNets. The analytical expressions are validated through extensive Monte Carlo simulations. We also study the impact of deploying mmWave small cells co-existing with traditional sub-6 GHz HetNet on the achievable EE, SE, and coverage probability. One of the key research finding is that the co-existence of mmWave and sub-6 GHz small cells overlaid with sub-6 GHz macrocell results in a significant improvement in spectral efficiency and coverage probability.
2) To the best of the authors' knowledge, the threefold tradeoff between EE, ASE, and outage probability has not yet been investigated in mmWave/sub-6 GHz hybrid K-tier HetNets. An optimization problem for computing the green efficient solution to maximize the EE under the minimum ASE and outage probability constraint is formulated and solved using convex optimization method. Various useful design insights are concluded from these findings, such as the fact that the increase in the BS density increases ASE and decreases the network EE, thus showing that network densification may not always result in the most efficient solution.
3) The inter-relationship between the coverage probability and network power consumption threshold is investigated in downlink transmission of mmWave/sub-6 GHz hybrid K-tier HetNets. Furthermore, the impact of this relationship on the achievable EE and ASE is analyzed.
4) We employ the exponential decay blockage model considering a two-state statistical model for each link. We use real building statistics obtained from the shape files of Chicago city (CC), USA, Lancaster University (LU), U.K., and NUST Campus (NC), Pakistan using the quantum geographic information system software to determine the blockage density. These three regions represent urban, suburban, and rural areas, respectively.
5) We investigate different deployment strategies to observe the impact of an increase in the mmWave BS density in mmWave/sub-6 GHz hybrid K-tier HetNets on the network power consumption in comparison to the traditional sub-6 GHz K-tier HetNet. Finally, we also analyze the impact of deliberately offloading users to a specific tier on the achievable network ASE.

The remainder of this paper is organized as follows. Section III introduces the system model, Section IV derives analytical expressions for association and coverage probability for both mmWave and sub-6 GHz tiers and corresponding numerical results are presented in Section V. Section V-A validates our model by comparing analytical results with simulation results, while Section V-B presents a detailed discussion of the effect of deployment parameters on the considered coverage probability and ASE. Section V-C investigates the tradeoff between ASE and EE subject to outage probability threshold, whereas Section V-D studies the tradeoff between coverage probability and network power consumption threshold. Finally, Section VI draws the conclusions of this paper.

III. System Model and Mathematical Preliminaries

A. Spatial Distributions

We consider the downlink transmission in a K-tier HetNet composed of sub-6 GHz macrocells overlaid with small cells operating at both sub-6 GHz and mmWave frequency bands, as shown in Fig. 1. The BSs of the kth tier are uniformly distributed in $\mathbb{R}^2$ and modeled as a 2-D homogeneous PPP Φ_k with intensity λ_k, where $k \in \mathcal{K} = \{1, 2, 3\}$. The users are also assumed to be uniformly distributed as a PPP Φ_{u} with intensity λ_{u} in $\mathbb{R}^2$. For better analytical tractability, we assume that all k-tier BSs have the same transmission power $\rho_{k,\mathrm{tx}}$, biasing factor θ_k and pathloss exponent (PLE) α_k. It should be noted that small cells operating at sub-6 GHz constitute tier 2, whereas the small cells operating in the mmWave frequency band form tier 3. The small cells operating in mmWave can be either LoS or NLoS to the user. Let Φ_3^{L} and Φ_3^{N} be the PPP of LoS and NLoS mmWave small cells obtained by applying independent thinning [27] on Φ_3 using the LoS probability function $p(R)$ to determine whether a link of length R is LoS or not. The intensities of Φ_3^{L} and Φ_3^{N} are subsequently determined by $p(R)\lambda_3$ and $(1 - p(R))\lambda_3$, respectively. λ_3 and $\lambda_{k_{\mathrm{mm}}}$ are interchangeably used for mmWave small cell tier throughout this paper.

We consider the maximum received power association scheme, which is formulated as follows:

$$\begin{aligned}\left(l^*{}_{\in\mathcal{K}}, m^*{}_{\in\Phi_l}\right) &= \arg\max\left(P_{k,t}\theta_k x_{k,t,n}^{-\alpha_k}\right)\\ &= \arg\max\left(P_k\theta_k x_{k,n}^{-\alpha_k}\right)\\ &\quad \forall k \in \mathcal{K};\ \forall t \in \Phi_k;\ \forall n \in \Phi_u \qquad (1)\\ \text{subject to:}\quad & y_{k,t,n} \in \{0,1\}\forall k \in \mathcal{K};\ \forall t \in \Phi_k;\ \forall n \in \Phi_u\\ & \sum_{k\in\mathcal{K}}\sum_{t\in\Phi_k} y_{k,t,n} = 1 \forall n \in \Phi_u \qquad (2)\end{aligned}$$

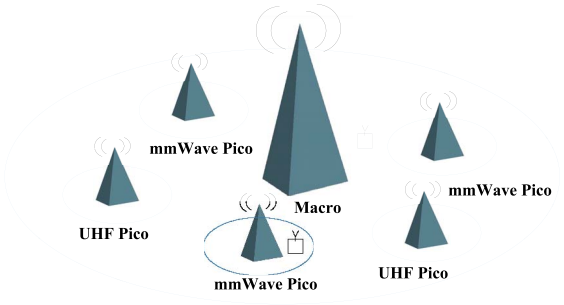

Fig. 1. System model of mmWave enabled 3-tier HetNet.

where $P_{k,t}$ is the transmission power of the tth BS of tier k normalized by its fixed pathloss given by $(4\pi/\lambda_c)^2$, λ_c as the carrier wavelength, and $x_{k,t,n}$ is the Euclidean distance of user n from the tth BS of tier k. Since each BS of tier k has the same transmission power, $P_{k,t} = P_k$ and $x_{k,t,n}$ becomes the distance of the user n from the closest kth tier BS $x_{k,n}$. $y_{k,t,n}$ is a binary indicator variable showing whether or not user n is served by the tth BS of tier k. For clarity purpose, we define

$$\hat{P_k} \triangleq \frac{P_k}{P_l}, \hat{\theta_k} \triangleq \frac{\theta_k}{\theta_l}, \text{ and } \hat{\alpha_k} \triangleq \frac{\alpha_k}{\alpha_l} \tag{3}$$

which are the normalized transmit power, biasing factor and PLE, respectively, of tier k conditioned that a user is associated with tier l.

Without loss of tractability, the analysis is carried out assuming a typical user to be located at origin O [27]. The SINR of a typical user at a distance x associated with its kth tier BS, for $k \in \{1, 2\}$ operating in sub-6 GHz can be expressed as

$$\text{SINR}_k = \gamma_k = \frac{P_k h_x x^{-\alpha_k}}{\sum_{k\in\{1,2\}} \sum_{i\in\Phi_k\setminus b_0} P_k h_i x_i^{-\alpha_k} + \sigma^2} \tag{4}$$

where $\sum_{k\in\{1,2\}} \sum_{i\in\Phi_k\setminus b_0} P_k h_i x_i^{-\alpha_k}$ is the total interference from macrocells or small cells operating in sub-6 GHz except for the serving BS b_0, h_x is the channel gain of the typical user at distance x from the serving BS and σ^2 is the noise power.

Similarly, the SINR of a typical user at distance x associated with its small cell operating in mmWave band can be expressed as

$$\text{SINR}_3 = \gamma_3 = \frac{P_3 M_r M_t h_x x^{-\alpha_3^{(j)}}}{P_3 \sum_{j\in\{L,N\}} \sum_{i\in\Phi_3^{(j)}\setminus b_0} G_l h_i x_i^{-\alpha_3^{(j)}} + \sigma^2} \tag{5}$$

where $j \in \{L, N\}$ shows if the interfering link is either LoS (L) or NLoS (N), M_t and M_r are the main lobe gains of the transmit and receive antennas, respectively, and G_l is the directivity gain of the interfering BSs. It is assumed that both the BSs and users are in perfect alignment such that the mmWave small cell is able to steer its antenna in the direction of a tagged user, whereas the user is also able to do the same for its tagged BS. Hence, the directivity gain of the desired signal link is given by $M_r M_t$. The beam direction of an interfering link is assumed to be independently and uniformly distributed in $(0, 2\pi]$. Similarly, the directivity gain of an interfering link denoted by G_l, where $l \in \{1, 2, 3, 4\}$ is given by

$$G_l = \begin{cases} G_1 = M_r M_t, \text{ with prob. } \Xi_1 = \left(\frac{\Theta_r}{2\pi}\frac{\Theta_t}{2\pi}\right) \\ G_2 = M_r m_t, \text{ with prob. } \Xi_2 = \left(\frac{\Theta_r}{2\pi}\left(1 - \frac{\Theta_t}{2\pi}\right)\right) \\ G_3 = m_r M_t, \text{ with prob. } \Xi_3 = \left(\left(1 - \frac{\Theta_r}{2\pi}\right)\frac{\Theta_t}{2\pi}\right) \\ G_4 = m_r m_t, \text{ with prob. } \Xi_4 = \left(\left(1 - \frac{\Theta_r}{2\pi}\right)\left(1 - \frac{\Theta_t}{2\pi}\right)\right) \end{cases}$$

where m_r and m_t are the receiver and transmitter side lobe gains, and Θ_r and Θ_t are the receiver and transmitter half power beamwidths, respectively.

B. Blockage Model

We use the same blockage model as the one used by Bai and Heath [9], given by

$$\Xi(R) = e^{-\beta R} \tag{6}$$

where R is the link distance and β is a parameter computed using statistics of the buildings. The parameter β is calculated as

$$\beta = \frac{-\chi \ln(1-\kappa)}{\pi A} \tag{7}$$

where A is the average area of the buildings in the considered region, κ is the fraction of the total area covered by buildings and χ is the average perimeter of the buildings in the considered region. The blockage parameters for CC (urban environment with dense blockages), LU (suburban environment), and NC (rural environment) are determined using the procedure outlined in [8]. These values, along with the environments, are shown in Fig. 2. The corresponding 2-D average LoS distance is given as

$$R_L = -\frac{(1-\kappa)\pi A}{\chi \ln(1-\kappa)}. \tag{8}$$

C. Performance Metrics and Tradeoffs

We consider the following performance metrics.

1) The SINR coverage probability for each tier k, defined as

$$\Xi_{c,k} = \mathbb{P}(\gamma_k > T) \tag{9}$$

where T is the SINR threshold. The aggregated coverage probability for the three-tier HetNets considered in Section III-A can be written as

$$\Xi_c(T) = \sum_{k=1}^{3} \xi_k \Xi_{c,k} \tag{10}$$

where ξ_k is the association probability that the typical user is associated with tier k. Similarly, the aggregated outage probability for three-tier HetNets can be defined as $\Xi_o = 1 - \Xi_c$.

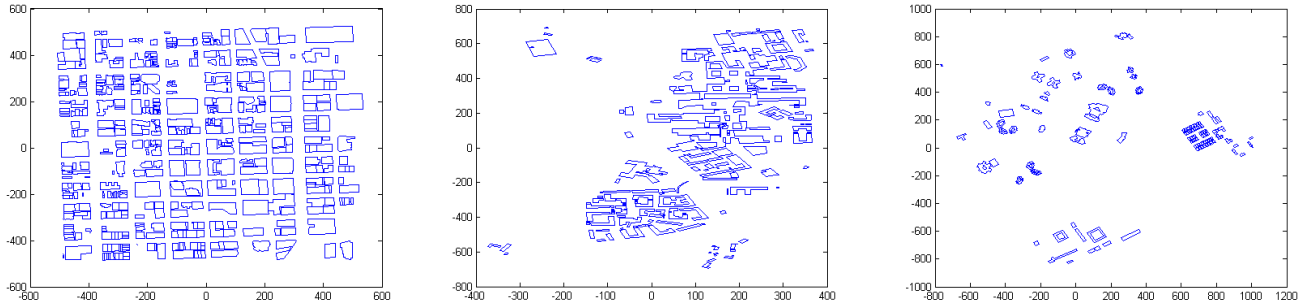

Fig. 2. Blockage scenarios under consideration. (a) CC, USA ($\beta = 0.0224$). (b) LU, U.K. ($\beta = 0.0057$). (c) NC, Pakistan ($\beta = 0.0014$).

2) The rate coverage probability for the kth tier $\Xi_k(R)$ can be computed using the SINR coverage probability $\Xi_{c,k}$ as in [16], as follows:

$$\mathbb{P}(R_k > r) = \mathbb{P}\left(\gamma_k > 2^{r/B_k} - 1\right) = \Xi_{c,k}\left(2^{r/B_k} - 1\right) \tag{11}$$

where r is the rate threshold and B_k is the signal bandwidth allocated to a user associated with the kth tier. Hence, similar to (9), the aggregated rate coverage probability is defined by

$$\Xi(R) = \sum_{k=1}^{3} \xi_k \Xi_{c,k}\left(2^{r/B_k} - 1\right). \tag{12}$$

3) We define the ASE Ω as the total rate in a unit area normalized by the bandwidth, given by

$$\Omega = \sum_{k=1}^{3} \lambda_k \Xi_{c,k}(T) \log_2(1+T) \tag{13}$$

where $\Xi_{c,k}(T)$ is the coverage probability conditioned on the user associated with the tier k and T is the SINR threshold. The unit of Ω is b/s/Hz/m^2.

4) We define the EE of the network denoted by η as follows:

$$\eta = \frac{\lambda_u \sum_{k=1}^{3} \xi_k B_k \log_2(1+T)\Xi_{c,k}(T)}{\sum_{k=1}^{3} \lambda_k \left(\frac{1}{\epsilon}\rho_{k,\text{tx}} + \rho_c\right)} \tag{14}$$

where ϵ is the amplifier efficiency and ρ_c is the load-independent circuit power.

Having listed the metrics used for analysis, we now move to some of the important tradeoffs that will be investigated during the course of this paper.

1) Tradeoff Between EE, ASE, and Outage Probability: The coverage probability in each tier k, i.e., $\Xi_{c,k}(T)$ is different, and increasing the individual tier BS density will have a different impact on the overall coverage probability $\Xi_c(T)$. From (12), it is quite obvious that Ω increases with an increase in λ_k. In order to achieve maximum Ω, it is optimal to activate all tiers, which in turn will result in a lower coverage probability $\Xi_c(T)$. Hence, we investigate the tradeoff between EE, ASE, and coverage probability for the proposed 3-tier model incorporating mmWave small cells co-existing with sub-6 GHz macrocells and small cells. Different from the previous works, the effect of an outage probability threshold is investigated on the achievable EE and ASE. We formulate an EE maximization problem subject to minimum ASE and outage probability requirement, as follows:

$$\begin{aligned} \textbf{P1:} \ & \max_{\lambda_k} \ \eta \\ & \text{s.t.} \ \ \Omega \geq \Omega^{\min} \\ & \quad (1 - \Xi_c(T)) \leq O_c^{\min}(T) \\ & \quad 0 \leq \lambda_k \leq \lambda_k^{\max} \forall k \in K \end{aligned} \tag{15a}$$

where $\Omega^{\min}$ is the minimum ASE requirement and $O_c^{\min}(T)$ is the minimum outage probability threshold at SINR target of T dB. It is worth mentioning that there is no feasible solution to this optimization problem if $O_c^{\min}(T) > (1 - \max_k \Xi_{c,k}(T))$ due to the fact that such coverage probability cannot be achieved irrespective of the tier BS density. This optimization problem is investigated for the case when $O_c^{\min}(T) \leq (1 - \max_k \Xi_{c,k}(T))$.

The problem **P1** is a nonlinear fractional problem which can be solved by using the Dinkelbach-type method [26] as follows:

$$G(\eta) = \max_{\underline{\lambda}} \left[E(\underline{\lambda}) - \eta F | \underline{\lambda} \in C\right] \overset{\text{(a)}}{=} \max_{\underline{\lambda}} \left[\overline{E}(\underline{\lambda}) - \eta^{(i)} F\right]$$

where $\underline{\lambda} = \{\lambda_1, \lambda_2, \ldots, \lambda_K\}$, $E(\underline{\lambda}) = \lambda_u \sum_{k=1}^{K} \xi_k B_k \log_2(1+T)\Xi_{c,k}(T)$, $F = \sum_{k=1}^{K} \lambda_k((1/\epsilon)\rho_{k,\text{tx}} + \rho_c)$, $C = \{\underline{\lambda} | \Omega \geq \Omega^{\min}, (1 - \Xi_c(T)) \leq O_c^{\min}(T), 0 \leq \lambda_k \leq \lambda_k^{\max}, \forall k \in K\}$ and the equality (a) follows by applying the sequential convex programming to approximate $E(\underline{\lambda})$ with the first-order Taylor expansion, such that $\overline{E}(\underline{\lambda}) = E(\underline{\lambda}^{(j)}) + \nabla E(\underline{\lambda}^{(j)})(\underline{\lambda} - \underline{\lambda}^{(j)})$ given the jth iterative $\underline{\lambda}^{(j)}$ and ith iterative $\eta^{(i)}$. The optimal $\underline{\lambda}^*$ can be found by obtaining η such that $G(\eta) = 0$, through standard convex optimization methods.

2) Tradeoff Between Coverage Probability and Network Power Consumption: The coverage probability P_c is analyzed as a function of network power consumption constraint for traditional HetNet with no mmWave small cells in comparison to our proposed 3-tier model incorporating mmWave small cells co-existing with sub-6 GHz macrocells and small cells. From this perspective, we have formulated an optimization problem to maximize the coverage probability subject to the network

power consumption constraint as follows:

$$\mathbf{P2:}\ \max_{\lambda_k}\ \Xi_c(T)$$
$$\text{s.t.}\ \sum_{k=1}^{K}\lambda_k\left(\frac{1}{\epsilon}\rho_{k,\text{tx}}+\rho_c\right)\leq\rho_{\max}$$
$$0\leq\lambda_k\leq\lambda_k^{\max}\forall k\in K \tag{15b}$$

where $\rho_{\max}$ is the maximum network power consumption constraint. The solution to **P2** is given by $\lambda_k^*=\min\{\lambda_k^0,\lambda_k^{\max},\overline{\lambda}_k\}$, where λ_k^0 can be found by taking the derivative of $\Xi_c(T)$ with respect to λ_k and setting it equal to zero and $\overline{\lambda}_k\leq(\rho_{\max}/[(1/\epsilon)(\rho_{k,\text{tx}}+\sigma_c)])^{(1/|K|)}$.

IV. Analysis of the Coverage Probability

We begin our analysis by presenting expressions for association and coverage probabilities. Detailed proofs have been omitted due to length constraints.

A. Association Probability

To obtain the aggregated coverage probability from (9) of the three-tier HetNet, we need to first derive the per-tier association probability ξ_k.

Lemma 1: The association probability that the user is associated with tier $k\in\{1,2\}$ is given as

$$\xi_k=2\pi\lambda_k\int_0^\infty x\exp\left(-\pi\sum_{k\in K\setminus k_{\text{mm}}}\lambda_k C_k x^{2/\hat{\alpha_k}}+J(x)\right)dx \tag{16}$$

and it follows that the association probability for the mmWave tier, or tier 3, is given by:

$$\xi_3=1-\sum_{k\in\{1,2\}}\xi_k \tag{17}$$

where $C_k=(\hat{P_k}\hat{\theta_k})^{(2/\alpha_k)}$ and $J(x)$ is the term that accounts for the mmWave tier and is given by

$$J(x)=\frac{2\pi\lambda_{k_{\text{mm}}}}{\beta^2}\left(e^{-\beta\left(\hat{P_3}\hat{\theta_3}\right)^{1/\alpha_L}x^{1/\hat{\alpha_L}}}+e^{-\beta\left(\hat{P_3}\hat{\theta_3}\right)^{1/\alpha_N}}\times x^{1/\hat{\alpha_N}}\left(\beta^2\left(\hat{P_3}\hat{\theta_3}\right)^{2/\alpha_N}x^{2/\hat{\alpha_N}}e^{\beta\left(\hat{P_3}\hat{\theta_3}\right)^{1/\alpha_N}x^{1/\hat{\alpha_N}}}+2\beta\left(\hat{P_3}\hat{\theta_3}\right)^{1/\alpha_N}x^{1/\hat{\alpha_N}}\right)\right). \tag{18}$$

B. mmWave Small Cell Tier Coverage

The SINR coverage probability of the mmWave small cell tier, given by $\Xi_{c,3}(T)$, is defined as the probability that the received SINR is greater than a certain threshold $T>0$, i.e., $\Xi_{c,3}(T)=\mathbb{P}(\gamma_3>T)$. As stated previously, the mmWave small cell BSs tier process Φ_3 can be divided into two independent PPPs: 1) the LoS small cell BS process Φ_3^L and 2) the NLoS small cell BS process Φ_3^N. Equivalently, Φ_3^L and Φ_3^N can be considered as two independent mmWave small cell BS tiers. Under the assumption of open access, a user will connect to the BS with the lowest pathloss. As a result, a user serviced by the mmWave small cell tier will connect to either the nearest LoS small cell BS or the nearest NLoS small cell BS.

The probability of a user being associated to an NLoS small cell BS, given that a user is being served by the mmWave small cell tier is

$$\begin{aligned}\xi_{3,N}&=\mathbb{P}\left[x_N^{-\alpha_N}>x_L^{-\alpha_L}\right]\\&=\mathbb{P}[x_L>\Delta_N(x)]\\&\overset{\text{(a)}}{=}\int_0^\infty\exp\{-2\pi\lambda_3\int_0^{\Delta_N(x)}tp(t)dt\}f_N(x)dx\end{aligned} \tag{19}$$

where $\Delta_N(x)=x^{\alpha_N/\alpha_L}$, equality (a) follows from (32), and $f_N(x)=(d/dx)(1-\mathbb{P}[x_N>\Delta_L(x)])=2\pi\lambda_3 x(1-p(x))\exp\{-2\pi\lambda_3\int_0^x(1-p(t))tdt\}$, with $\mathbb{P}[x_N>\underbrace{\Delta_L(x)}_{x}]=\exp\{-2\pi\lambda_3\int_0^x(1-p(t))tdt\}$ obtained by the following [9, Lemma 2], and $\Delta_L(x)=x^{\alpha_L/\alpha_N}$.

Given that a user is served by an NLoS small cell BS, the probability density function (PDF) of its distance to the serving BS is

$$\hat{f}_N(x)\overset{\text{(a)}}{=}\frac{2\pi\lambda_3 x(1-\Xi(x))e^{\{-2\pi\lambda_3\int_0^x(1-\Xi(t))tdt\}}e^{\left\{-2\pi\lambda_3\int_0^{\Delta_N(x)}t\Xi(t)dt\right\}}}{\xi_{3,N}} \tag{20}$$

where (a) follows from Lemma 1 and (18), and $\Xi(.)$ is the LoS probability function defined in (5). Detailed steps about computing the PDF are outlined in Lemma 2. The probability that a user is associated with an LoS small cell BS is given by $\xi_{3,L}=1-\xi_{3,N}$. Similarly, for a user that is served by an LoS small cell BS, the PDF of its distance to the serving small cell BS is

$$\hat{f}_L(x)=\frac{2\pi\lambda_3 x\Xi(x)e^{\{-2\pi\lambda_3\int_0^x t\Xi(t)dt\}}e^{\left\{-2\pi\lambda_3\int_0^{\Delta_L(x)}(1-\Xi(t))tdt\right\}}}{\xi_{3,L}}. \tag{21}$$

Finally, we derive the expression for the overall coverage probability for users associated with the mmWave tier, given in the following theorem.

Theorem 1: The SINR coverage probability $\Xi_{c,3}(T)$ of users associated with the mmWave small cell tier is

$$P_{c,3}(T)=\sum_{j\in\{L,N\}}\xi_{3,j}\Xi_{c,3}^{(j)} \tag{22}$$

where $\Xi_{c,3}^{(L)}(T)$ and $\Xi_{c,3}^{(N)}(T)$ are the conditional coverage probabilities when a user, associated with the mmWave small cell tier, forms a link with a small cell BS in Φ_3^L and Φ_3^N, respectively. Subsequently, $\Xi_{c,3}^{(L)}(T)$ can be evaluated by

$$\Xi_{c,3}^{(j)}(T)=\int_0^\infty\exp\left(-\frac{x^{\alpha_j}T\sigma^2}{P_3M_rM_t}-B_j(T,x)\right)\hat{f}_j(x)dx \tag{23}$$

where $B_j(T,x)$ are shown at the bottom of the next page in (24a) and (24b) and $\hat{f}_j(x),\forall j\in\{L,N\}$ is given in (20) and (21). For $l\in\{1,2,3,4\}$, $\bar{a}_l=(M_l/M_rM_t)$, where M_l and Ξ_l are constants defined in G_l, as outlined in Section III-A.

A particular case of the above theorem can be obtained by making the substitution $I_L = I_N = 0$, which follows from the fact that $\sigma^2 \gg I_L + I_N$ in noise-limited mmWave networks. In this case, we have

$$\Xi_{c,3}^{(L)}(T) = \frac{2\pi\lambda_3}{\xi_{3,L}} \int_0^\infty x\Xi(x)\exp\left\{ \frac{-x^{\alpha_L}\sigma^2 T}{P_k M_r M_t} - 2\pi\lambda_3 \times \int_0^x t\Xi(t)dt - 2\pi\lambda_3 \times \int_0^{\Delta_L(x)} t(1-\Xi(t))dt \right\} dx \tag{25a}$$

$$\Xi_{c,3}^{(N)}(T) = \frac{2\pi\lambda_3}{\xi_{3,N}} \int_0^\infty (1-x)\Xi(x) \times \exp\left\{ \frac{-x^{\alpha_N}\sigma^2 T}{P_k M_r M_t} - 2\pi\lambda_3 \times \int_0^x t(1-\Xi(t))dt - 2\pi\lambda_3 \times \int_0^{\Delta_N(x)} t\Xi(t)dt \right\} dx. \tag{25b}$$

C. Sub-6 GHz and Aggregate Network Coverage

Prior to deriving the expressions for coverage of sub-6 GHz cells, we present the following lemma.

Lemma 2: The PDF $f_{X_k}(x)$ of the distance X_k between a typical user and its serving sub-6 GHz AP, i.e., $k \in K \setminus k_{\text{mm}}$ is given by

$$f_{X_k}(x) = \frac{2\pi\lambda_k}{\xi_k} x \exp\left\{ -\pi \sum_{j=1}^{2} \lambda_j C_j x^{2/\hat{\alpha}_j} + J(x) \right\} \tag{26}$$

where ξ_k is defined in (15) and $J(x)$ is defined in (17). We now present the theorem for aggregate network coverage.

Theorem 2: The aggregate network coverage $\Xi_c(T)$ can be computed as

$$\Xi_c(T) = \sum_{k \in K \setminus 3} \xi_k \Xi_{c,k}(T) + \xi_3 \Xi_{c,3}(T) \tag{27}$$

where $\Xi_{c,3}(T)$ is defined in Theorem 1. Furthermore $\Xi_{c,k}(T)$, where $k \in \{1, 2\}$, is given by

$$\Xi_{c,k} = \int_0^\infty \exp\left\{ \frac{-Tx^{\alpha_k}\sigma^2}{P_k} - \delta_1 - \delta_2 \right\} f_{X_k}(x)dx \tag{28}$$

where

$$\delta_1 = \pi\lambda_1 \hat{P}_1^{2/\alpha_1} x^{2/\hat{\alpha_1}} Z\left(T, \alpha_1, \hat{\theta}_1\right) \tag{29}$$

$$\delta_2 = \pi\lambda_2 \hat{P}_2^{2/\alpha_2} x^{2/\hat{\alpha_2}} Z\left(T, \alpha_2, \hat{\theta}_2\right) \tag{30}$$

TABLE I
PARAMETER VALUES

Parameter	Symbol	Numerical value (unless stated otherwise)
Sub-6 GHz bandwidth	B_1, B_2	20 MHz
mmWave bandwidth	B_3	100 MHz
Amplifier efficiency	ϵ	0.9
Circuit power	ρ_c	0.1 W
Transmit power of k^{th} tier normalized by fixed pathloss (W)	P_k	$P_1 = 0.0039$ $P_2 = 9.895 \times 10^{-5}$ $P_3 = 7.27 \times 10^{-7}$
Receiver main lobe gain, side lobe gain and beam width	M_r, m_r, Θ_r	$M_r = 10$ dB $m_r = -10$ dB $\Theta_r = 90^{\text{o}}$
Transmitter main lobe gain, side lobe gain, beam width	M_t, m_t, Θ_t	$M_t = 20$ dB $m_t = -10$ dB $\Theta_t = 30^{\text{o}}$

and

$$Z(T, \alpha, \theta) = T^{2/\alpha} \int_{\left(\frac{\theta}{T}\right)^{2/\alpha}}^\infty \frac{dv}{1 + v^{\frac{\alpha}{2}}}. \tag{31}$$

If we substitute $\sigma^2 = 0$, which is a fair assumption given that the sub-6 Hz networks are typically interference-limited and $\alpha_1 = \alpha_2$, considerable simplification follows:

$$\Xi_{c,k}(T) = \int_0^\infty \exp\left\{ -x^2 \sum_{j=1}^{2} \pi\lambda_j \sqrt{T\hat{P}_k} \left(\frac{\pi}{2} - \arctan\sqrt{\frac{\hat{\theta}_k}{T}} \right) + \frac{2\pi}{\lambda_k} x \exp\left\{ -\pi x^2 \sum_{j=1}^{2} \lambda_j C_j - 2\pi\lambda_3 \times \left[\int_0^{\frac{P_3\theta_3}{P_k\theta_k}^{1/\alpha_L} x^{4/\alpha_L}} x e^{-\beta x} + \int_0^{\frac{P_3\theta_3}{P_k\theta_k}^{1/\alpha_N} x^{4/\alpha_N}} x \times (1 - e^{-\beta x}) \right] \right\} \right\}. \tag{32}$$

$$B_L(T, x) = 2\pi\lambda_{k_{\text{mm}}} \sum_{l=1}^{4} p_l \left[\int_x^\infty \frac{1}{1 + \left(Tx^{\alpha_L} t^{-\alpha_L} \bar{a}_l\right)^{-1}} tp(t)dt + \int_{\Delta_L(x)}^\infty \frac{1}{1 + \left(Tx^{\alpha_L} t^{-\alpha_N} \bar{a}_l\right)^{-1}} t(1-p(t))dt \right] \tag{24a}$$

$$B_N(T, x) = 2\pi\lambda_{k_{\text{mm}}} \sum_{l=1}^{4} p_l \left[\int_{\Delta_N(x)}^\infty \frac{1}{1 + \left(Tx^{\alpha_N} t^{-\alpha_L} \bar{a}_l\right)^{-1}} tp(t)dt + \int_x^\infty \frac{1}{1 + \left(Tx^{\alpha_N} t^{-\alpha_N} \bar{a}_l\right)^{-1}} t(1-p(t))dt \right] \tag{24b}$$

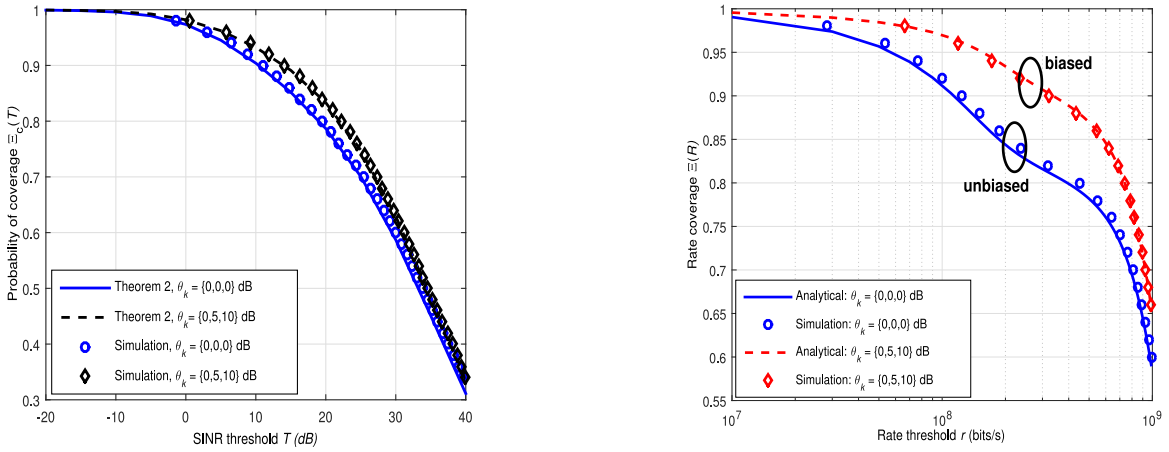

Fig. 3. Effect of varying the biasing factor θ_k on the coverage and rate probabilities with $\lambda_1 = \lambda_0$, $\lambda_2 = \lambda_3 = 30\lambda_0$. The lines represent analytical curves while the markers are simulation results. (a) Coverage probability $\Xi_c(T)$ versus SINR threshold T. (b) Rate coverage $\Xi(R)$ versus rate threshold r.

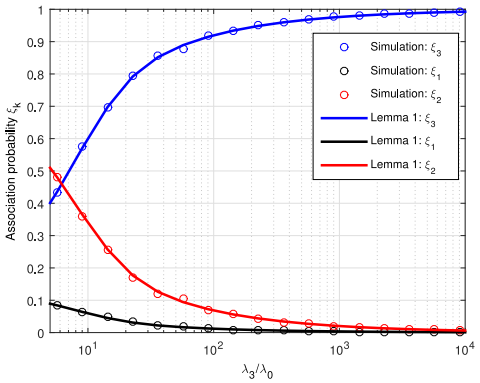

Fig. 4. Unbiased association probability ξ_k versus the relative mmWave small cell BS density λ_3/λ_0.

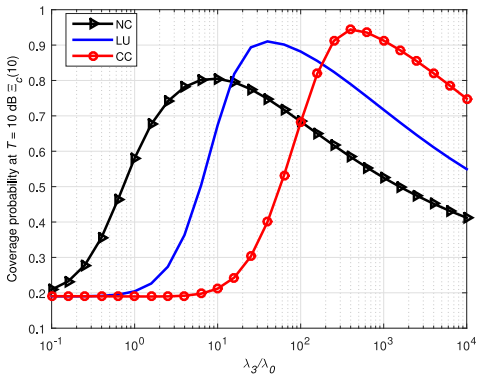

Fig. 5. Impact of varying tier 3 BS density on the coverage probability with $\theta_1 = \theta_2 = \theta_3 = 0$ dB for three real buildings blockage model consisting of: CC, LU, and NC. Here, $\lambda_1 = \lambda_0$ and $\lambda_2 = 30\lambda_0$.

V. Numerical Results

A. Model Accuracy and Analysis

In this paper, we assume that the mmWave and sub-6 GHz operating frequencies are 28 and 2.4 GHz, respectively. We use the term intersite distance $r_{d,k}$ to define the BS deployment density. We define λ_0 such that $r_{d,0} = 1000$ m and use it as a basis to determine individual tier BS densities. We also assume that the sub-6 GHz PLE is 4 and the mmWave LoS and NLoS PLEs are 2 and 4, respectively. Unless otherwise specified, values for the different parameters used in this section are given in Table I. We use Monte Carlo simulations, using PPP deployment, to verify the presented model. A single user is deployed at the origin in each iteration and its SINR is calculated using channel gains generated from an exponential distribution with mean 1. We employ 10 000 trials in order to generate ergodic simulation results.

Fig. 3(a) shows the biased and unbiased network coverage. The graphs show that offloading users to small cells improves the SINR coverage of the network. Furthermore, we can notice that the analytical results are close to the simulation ones, which validates our model. The graphs in Fig. 3(b) show the biased and unbiased rate coverage probabilities $\Xi(R)$ as a function of the rate threshold, r. We can observe that the biased network shows greater rates as opposed to the unbiased network, which is natural given the greater bandwidth allotted to users associated with mmWave BSs. We can also see that simulation results match the trend generated using (12).

Fig. 4 shows the relationship between the tier association probabilities ξ_k and varying mmWave BS density λ_3. Results show that ξ_3 increases as λ_3 increases. This follows from the fact that the average cell radius is reduced which allows for greater probabilites of LoS links being formed. The macrocell association is significantly lower due to sparse deployments. The figure also shows that simulation results match those obtained using Lemma 1.

B. Effect of BS Density and Biasing Factor on Coverage Probability and ASE

In this section, we analyze the impact of the BS density and biasing factor on the performance metrics considered in this paper. This analysis is conducted for three different blockage environments: 1) CC (urban environment with dense blockages); 2) LU (suburban environment); and 3) NC (rural environment).

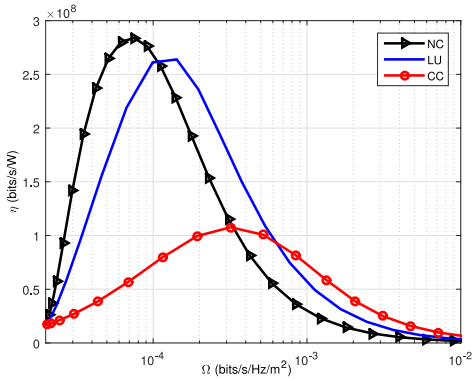

Fig. 6. Tradeoff between ASE and EE in an unbiased network with $\lambda_3^{\max} = 9.5493 \times 10^{-3}$ per m^2. In this figure, an optimal λ_3^* is found with $\lambda_1 = \lambda_0$, $\lambda_2 = 30\lambda_0$, $\lambda_u = 100$ users/km^2 $\epsilon = 90\%$, and $\rho_c = 0.1$ W.

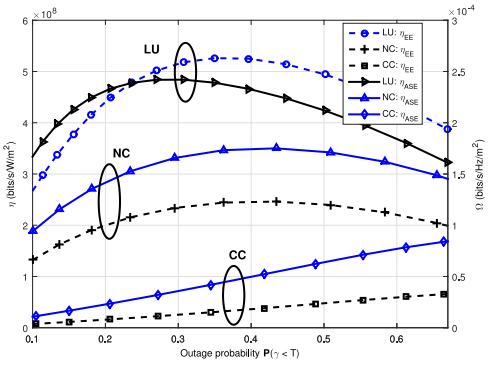

Fig. 7. ASE and EE versus outage probability for an unbiased network when $\lambda_1 = \lambda_0$, $\lambda_2 = \lambda_3 = 30\lambda_0$, and $\lambda_u = 100$ users/km^2. In this figure, a load-independent power ρ_c of 0.1 W and an amplifier efficiency ϵ of 0.9 are considered.

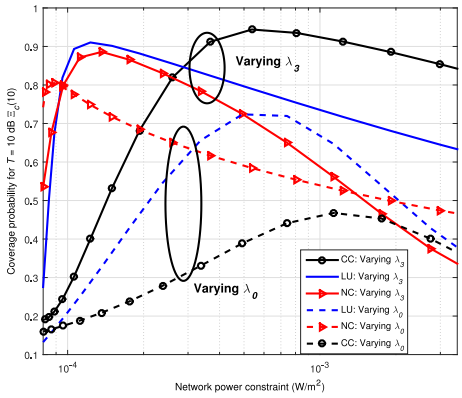

Fig. 8. Coverage probability versus network power consumption for an unbiased network. In the first strategy (optimal λ_3^* is found), $\lambda_1 = \lambda_0$, $\lambda_2 = 30\lambda_0$, and $\lambda_3^{\max} = 9.5493 \times 10^{-3}$ per m^2. In the second strategy (optimal λ_0^* is found), $\lambda_1 = \lambda_0$, $\lambda_2 = \lambda_3 = 30\lambda_0$, and $\lambda_0^{\max} = 9.5493 \times 10^{-3}$ per m^2.

Fig. 5 shows the relation between the coverage probability at an SINR threshold $T = 10$ dB and λ_3/λ_0, where λ_0 is fixed. The graph shows that increasing BS density yields better coverage only for relatively sparse deployments. An optimum density exists, which depends on the environment. The CC area has the greatest optimum mmWave BS density of $\lambda_3 = 300\lambda_0$ followed by LU, with $\lambda_3 = 30\lambda_0$ and finally the NC with an optimum BS density of $\lambda_3 = 6\lambda_0$. The trends show that as the density of blockages increases, the optimal mmWave cell radius decreases. This follows from the fact that the LoS probability function decays exponentially with increasing blockages.

C. Tradeoff Between ASE and EE Subject to Outage Probability Threshold

In this section, we analyze the impact of the outage probability threshold on the achievable EE and ASE. Fig. 6 shows the tradeoff between ASE and EE in an unbiased network. The network ASE increases with increasing λ_3. However, the network power consumption increases with increasing BSs, hence a tradeoff occurs between ASE and EE. Networks deployed in environments with sparse blockages show greater maximum EE when compared to those deployed in urban settings. In suburban or rural settings, a less dense mmWave BS deployment is required to achieve better coverage, and hence, better rates. As a result, the power required to maintain those data rates is lower and the maximum EE is greater. The result also shows an environment dependent EE profile, which follows from our result in Fig. 5.

Fig. 7 shows the trend between EE and ASE subject to the outage probability constraint $\mathbb{P}(\gamma < T)$. The curves are generated by changing the SINR threshold, and determining the outage probability, ASE and EE for each value of T. Results show that the ASE increases as the outage increases up to a certain point, after which it gradually decreases. The trend is explained by (13), which outlines the dependence of ASE on the coverage probability. The ASE increases as long as the term $\log_2(1+T)$ is dominant. However, at larger SINR thresholds, the decrease in the coverage probability becomes dominant, and thus, the ASE decreases. The network EE versus outage probability follows a similar trend as the ASE. This is evident from similarity of the numerator in (13) to the one in (12).

D. Coverage Probability Versus Network Power Consumption Threshold

Here, we investigate the effect of network power consumption on the coverage probability in the three-tier HetNet.

Fig. 8 shows the optimum coverage for a given network power constraint using two deployment strategies. In the first strategy, λ_1 and λ_2 are fixed, and the optimal mmWave small cell density λ_3^* is found. The second strategy increases the BS density of the entire network by increasing λ_0. Since λ_1, λ_2, and λ_3 are integer multiples of λ_0 the entire network deployment becomes denser. The network power consumption is calculated as $\rho_{\text{net}} = \sum_{k=1}^{3} \lambda_k((1/\epsilon)\rho_{k,\text{tx}} + \rho_c)$. The curves show that increasing the density of all tiers of the network leads to poorer gains in coverage regardless of the environment. This is because there is no significant decrease in user association with sub-6 GHz cells but there is significant increase in interference. Increasing only the mmWave

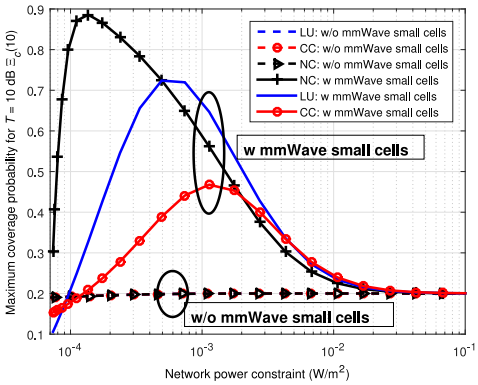

Fig. 9. Coverage probability at an SINR threshold of 10 dB versus network power constraint for network with $\lambda_3 = 30\lambda_0$ and without mmWave small cells. In this case, the optimal λ_0^* is found with $\lambda_1 = \lambda_0$, $\lambda_2 = 30\lambda_0$, and $\lambda_0^{\max} = 9.5493 \times 10^{-3}$ per m^2.

BS density also leads to lower energy consumption than in the previous case.

Fig. 9 depicts the coverage probability versus the network power constraint at a given SINR threshold for the proposed HetNet model in comparison to the traditional sub-6 GHz HetNet model with no small cells operating in mmWave band. It can be seen that at the given SINR threshold, the coverage probability for the sub-6 GHz only network does not increase beyond 0.2 regardless of the power constraint. Results show that sub-6 GHz networks generally show lower coverage probabilities at SINR threshold of 10 dB than the networks with mmWave small cells. This stems from the fact that the mmWave links are noise limited and improved SINRs can be achieved through the use of directional antenna. This leads to improved coverage probabilities.

VI. Conclusion

We analyzed propagation models for coverage in HetNets with both mmWave and sub-6 GHz small cells, and subsequently used them to study various performance metrics of the network. Then, we considered a variety of blockage environments to sustain the tractability of the analysis. The effects of the deployment parameters, such as BS density, on coverage probability, rate, spectral efficiency, and EE were studied. Through rigorous analysis, we concluded that introducing mmWave small cells considerably improves coverage and hence spectral efficiency. It was also seen that deployment strategies need to be devised keeping the environment in mind. Simulation results support the analytical findings.

References

[1] T. S. Rappaport *et al.*, "Millimeter wave mobile communications for 5G cellular: It will work!" *IEEE Access*, vol. 1, pp. 335–349, 2013.

[2] X. Ge *et al.*, "Spatial spectrum and energy efficiency analysis of random cellular networks," *IEEE Trans. Commun.*, vol. 63, no. 3, pp. 1019–1030, Jan. 2015.

[3] S. A. R. Naqvi and S. A. Hassan, "Combining NOMA and mmWave technology for cellular communication," in *Proc. IEEE Veh. Technol. Conf. (VTC Fall)*, Montreal, QC, Canada, Sep. 2016, pp. 1–5.

[4] X. Ge, S. Tu, T. Han, Q. Li, and G. Mao, "Energy efficiency of small cell backhaul networks based on Gauss–Markov mobile models," *IET Netw.*, vol. 4, no. 2, pp. 158–167, Mar. 2015.

[5] M. Xiao *et al.*, "Millimeter wave communications for future mobile networks," *IEEE J. Sel. Areas Commun*, vol. 35, no. 9, pp. 1909–1935, Sep. 2017.

[6] M. Ding, P. Wang, D. López-Pérez, G. Mao, and Z. Lin, "Performance impact of LoS and NLoS transmissions in dense cellular networks," *IEEE Trans. Wireless Commun.*, vol. 15, no. 3, pp. 2365–2380, Mar. 2016.

[7] S. Rangan, T. S. Rappaport, and E. Erkip, "Millimeter-wave cellular wireless networks: Potentials and challenges," *Proc. IEEE*, vol. 102, no. 3, pp. 366–385, Mar. 2014.

[8] M. N. Kulkarni, S. Singh, and J. G. Andrews, "Coverage and rate trends in dense urban mmWave cellular networks," in *Proc. IEEE Glob. Commun. Conf. (GLOBECOM)*, Austin, TX, USA, 2014, pp. 3809–3814.

[9] T. Bai and R. W. Heath, "Coverage and rate analysis for millimeter-wave cellular networks," *IEEE Trans. Wireless Commun.*, vol. 14, no. 2, pp. 1100–1114, Feb. 2015.

[10] J. G. Andrews, F. Baccelli, and R. K. Ganti, "A tractable approach to coverage and rate in cellular networks," *IEEE Trans. Commun.*, vol. 59, no. 11, pp. 3122–3134, Nov. 2011.

[11] Y. Hao, Q. Ni, H. Li, and S. Hou, "On the energy and spectral efficiency tradeoff in massive MIMO-enabled HetNets with capacity-constrained backhaul links," *IEEE Trans. Commun.*, vol. 65, no. 11, pp. 4720–4733, Nov. 2017.

[12] A. Ijaz, S. A. Hassan, S. A. R. Zaidi, D. N. K. Jayakody, and S. M. H. Zaidi, "Coverage and rate analysis for downlink HetNets Using modified reverse frequency allocation scheme," *IEEE Access*, vol. 5, pp. 2489–2502, 2017.

[13] Z. Zhang, Z. Ma, M. Xiao, G. Liu, and P. Fan, "Modeling and analysis of non-orthogonal MBMS transmission in heterogeneous networks," *IEEE J. Sel. Areas Commun.*, vol. 35, no. 10, pp. 2221–2237, Oct. 2017.

[14] H.-S. Jo, Y. J. Sang, P. Xia, and J. G. Andrews, "Heterogeneous cellular networks with flexible cell association: A comprehensive downlink SINR analysis," *IEEE Trans. Wireless Commun.*, vol. 11, no. 10, pp. 3484–3495, Oct. 2012.

[15] R. W. Heath, M. Kountouris, and T. Bai, "Modeling heterogeneous network interference using Poisson point processes," *IEEE Trans. Signal Process.*, vol. 61, no. 16, pp. 4114–4126, Aug. 2013.

[16] S. Singh, M. N. Kulkarni, A. Ghosh, and J. G. Andrews, "Tractable model for rate in self-backhauled millimeter wave cellular networks," *IEEE J. Sel. Areas Commun.*, vol. 33, no. 10, pp. 2196–2211, Oct. 2015.

[17] J. Park, S.-L. Kim, and J. Zander, "Tractable resource management with uplink decoupled millimeter-wave overlay in ultra-dense cellular networks," *IEEE Trans. Wireless Commun.*, vol. 15, no. 6, pp. 4362–4379, Jun. 2016.

[18] O. W. Bhatti *et al.*, "Performance analysis of decoupled cell association in multi-tier hybrid networks using real blockage environments," in *Proc. IEEE Int. Wireless Commun. Mobile Compt.*, Valencia, Spain, Jun. 2017, pp. 62–67.

[19] A. Umer, S. A. Hassan, H. B. Parveiz, Q. Ni, and L. Musavian, "Coverage and rate analysis for massive MIMO-enabled heterogeneous networks with millimeter wave small cells," in *Proc. IEEE Veh. Technol. Conf. (VTC Spring)*, Sydney, NSW, Australia, Jun. 2017, pp. 1–5.

[20] M. S. Omar, M. A. Anjum, S. A. Hassan, H. Pervaiz, and Q. Ni, "Performance analysis of hybrid 5G cellular networks exploiting mmWave capabilities in suburban areas," in *Proc. IEEE Int. Conf. Commun. (ICC)*, Kuala Lumpur, Malaysia, May 2016, pp. 1–6.

[21] E. Bedeer, O. A. Dobre, M. H. Ahmed, and K. E. Baddour, "A multiobjective optimization approach for optimal link adaptation of OFDM-based cognitive radio systems with imperfect spectrum sensing," *IEEE Trans. Wireless Commun.*, vol. 13, no. 4, pp. 2339–2351, Apr. 2014.

[22] O. Amin, E. Bedeer, M. H. Ahmed, and O. A. Dobre, "Energy efficiency–spectral efficiency tradeoff: A multiobjective optimization approach," *IEEE Trans. Veh. Technol.*, vol. 65, no. 4, pp. 1975–1981, Apr. 2016.

[23] L. Zhang *et al.*, "Performance analysis and optimization in downlink NOMA systems with cooperative full-duplex relaying," *IEEE J. Sel. Areas Commun.*, vol. 35, no. 10, pp. 2398–2412, Oct. 2017.

[24] Z. Zhang *et al.*, "Non-orthogonal multiple access for cooperative multicast millimeter wave wireless networks," *IEEE J. Sel. Areas Commun.*, vol. 35, no. 8, pp. 1794–1808, Aug. 2017.

[25] G. Yang, J. Du, and M. Xiao, "Maximum throughput path selection with random blockage for indoor 60 GHz relay networks," *IEEE Trans. Commun.*, vol. 63, no. 10, pp. 3511–3524, Oct. 2015.

[26] W. Dinkelbach, "On nonlinear fractional programming," *Manag. Sci.*, vol. 13, no. 7, pp. 492–498, Mar. 1967. [Online]. Available: http://www.jstor.org/stable/2627691
[27] F. Baccelli and B. Blaszczyszyn, *Stochastic Geometry and Wireless Networks, Volume 1—Theory*. Boston, MA, USA: NOW, 2009.

Muhammad Shahmeer Omar (S'16–M'16) received the B.Eng. degree in electrical engineering from the National University of Sciences and Technology, Islamabad, Pakistan, in 2015. He is currently pursuing the master's degree in electrical and computer engineering at the Georgia Institute of Technology, Atlanta, GA, USA.

His current research interests include 5G networks and millimeter wave communications.

Syed Ali Hassan (GS'08–M'11–SM'17) received the B.E. degree in electrical engineering (Highest Hons.) from the National University of Sciences and Technology (NUST), Islamabad, Pakistan, in 2004, the M.S. degree in electrical engineering from the University of Stuttgart, Stuttgart, Germany, in 2007, the M.S. degree in mathematics from the Georgia Institute of Technology, Atlanta, GA, USA, in 2011, and the Ph.D. degree in electrical engineering from the Georgia Institute of Technology, in 2011.

He is currently an Assistant Professor with the School of Electrical Engineering and Computer Science, NUST, where he is the Director of Information Processing and Transmission Research Group, which focuses on various aspects of theoretical communications. His current research interest includes signal processing for communications.

Haris Pervaiz (GS'09–M'09) received the M.Sc. degree in information security from the Royal Holloway University of London, Egham, U.K., in 2005, and the Ph.D. degree from the School of Computing and Communication, Lancaster University, Lancaster, U.K., in 2016.

He is currently a Research Fellow with the 5G Innovation Centre, University of Surrey, Guildford, U.K. From 2016 to 2017, he was an EPSRC Doctoral Prize Fellow with the School of Computing and Communication, Lancaster University. His current research interests include green heterogeneous wireless communications and networking, 5G and beyond, millimeter wave communication, and energy and spectral efficiency.

Qiang Ni (M'04–SM'08) received the B.Sc., M.Sc., and Ph.D. degrees from the Huazhong University of Science and Technology, Wuhan, China, all in engineering.

He led the Intelligent Wireless Communication Networking Group, Brunel University, London, U.K. He is currently a Professor and the Head of the Communication Systems Group, InfoLab21, School of Computing and Communications, Lancaster University, Lancaster, U.K. His current research interests include wireless communications and networking, including green communications, cognitive radio systems, 5G, IoT, and vehicular networks.

Dr. Ni was an IEEE 802.11 Wireless Standard Working Group voting member and a contributor to IEEE wireless standards.

Leila Musavian (S'05–M'07) received the Ph.D. degree in telecommunications from King's College London, London, U.K., in 2006.

She was a Lecturer with InfoLab21, Lancaster University, Lancaster, U.K., from 2012 to 2016. She is currently a Reader with the School of Computer Science and Electrical Engineering, University of Essex, Colchester, U.K. She was a Research Associate with McGill University, Montreal, QC, Canada, from 2011 to 2012, and a Post-Doctoral Fellow with INRS-EMT, Montreal, from 2006 to 2008. Her current research interests include radio resource management for next generation wireless networks, CRNs, energy harvesting, green communication, energy-efficient transmission techniques, cross-layer design for delay QoS provisioning, and 5G systems.

Dr. Musavian is an Editor of the IEEE TRANSACTIONS ON WIRELESS COMMUNICATIONS, an Executive Editor of *Transactions on Emerging Telecommunications Technologies* and an Associate Editor of *Internet Technology Letters* (Wiley).

Shahid Mumtaz (M'13–SM'16) received the M.Sc. degree in electrical and electronic engineering from the Blekinge Institute of Technology, Karlskrona, Sweden, in 2006, and the Ph.D. degree in electrical and electronic engineering from the University of Aveiro, Aveiro, Portugal, in 2011.

He was a Research Intern with Ericsson, Stockholm, Sweden, and Huawei Research Laboratory, Karlskrona, Sweden, in 2005. He has more than ten years of wireless industry experience and is currently a Senior Research Scientist and the Technical Manager with the Instituto de Telecommuninições Aveiro, Aveiro, Portugal. He has authored/co-authored over 100 publications in international conferences, journal papers, and book chapters. His current research interests include field of architectural enhancements to 3GPP networks (i.e., LTE-A user plan and control plan protocol stack, NAS, and EPC), 5G-related technologies, green communications, cognitive radio, cooperative networking, radio resource management, cross-layer design, backhaul/fronthaul, heterogeneous networks, machine-to-machine and device-to-device communication, and baseband digital signal processing.

Octavia A. Dobre (M'05–SM'07) received the Engineering Diploma and Ph.D. degrees from the Politehnica University of Bucharest (formerly the Polytechnic Institute of Bucharest), Bucharest, Romania, in 1991 and 2000, respectively.

In 2002 and 2005, she was with the Politehnica University of Bucharest and the New Jersey Institute of Technology, Newark, NJ, USA. In 2005, she joined Memorial University, St. John's, NL, Canada, where she is currently a Professor and the Research Chair. She was a Visiting Professor with the Université de Bretagne Occidentale, Brest, France, and the Massachusetts Institute of Technology, Cambridge, MA, USA, in 2013. Her current research interests include 5G enabling technologies, blind signal identification and parameter estimation techniques, cognitive radio systems, as well as optical and underwater communications among others.

Dr. Dobre was a recipient of the Royal Society Scholarship at Westminster University, U.K., in 2000, and the Fulbright Fellowship with the Stevens Institute of Technology, USA, in 2001. She serves as the Editor-in-Chief of *IEEE Communications Letters*, as well as an Editor of IEEE SYSTEMS JOURNAL, and IEEE COMMUNICATIONS SURVEYS AND TUTORIALS. She was an Editor and a Senior Editor of *IEEE Communications Letters*, an Editor of the IEEE TRANSACTIONS ON WIRELESS COMMUNICATIONS, and a Guest Editor of other journals. She served as the General Chair, the Tutorial Co-Chair, and the Technical Co-Chair at numerous conferences. She is the Chair of the IEEE ComSoc Signal Processing and Communications Electronics Technical Committee, as well as a Member-at-Large of the Administrative Committee of the IEEE Instrumentation and Measurement Society. She is a Fellow of the Engineering Institute of Canada.